Acupoint Injection of Dextrose Attenuates Chronic Inflammatory Pain In Mice Through Modulation of Transient Receptor Potential V1 Channel Expression

Hsien-Yin Liao
School of Post-Baccalaureate Chinese Medicine
Ming-Chia Lin
Department of necleur medicine, I-da University
Yi-Wen Lin (yiwenlin@mail.cmu.edu.tw)
Graduate institute of acupuncture science https://orcid.org/0000-0001-7204-8837

Research

Keywords: Prolotherapy, Chronic inflammatory pain, Acupoint injection TRPV1, Iba1

Posted Date: May 6th, 2021

DOI: https://doi.org/10.21203/rs.3.rs-472766/v1

Abstract

Background: Neuroinflammatory processes initiated by injury, infection, and other insults induce long-term alterations in the signaling characteristics of nociceptive neurons and associated non-neuronal cells, resulting in chronic inflammatory pain (CIP). Prolotherapy, also termed acupoint injection (AI) therapy, utilizes anatomically based meridians derived from Chinese Medicinal Theory to attenuate chronic pain. In fact, AI has demonstrated superior results compared to traditional acupuncture methods without significant side effects.

Methods: In this study, we explored the efficacy and underlying mechanisms of AI on CIP in mice. The mouse hindpaw was injected with complete Freund's adjuvant (CFA) to induce CIP, followed AI treatment.

Results: After two weeks, indices of mechanical and thermal hyperalgesia were significantly reduced by AI treatment. CIP was associated with elevated expression levels of transient receptor potential V1 (TRPV1) channels, various downstream kinases and transcription factors, and nociception-associated voltage-gated sodium channels ($Na_V s$) in dorsal root ganglion (DRG), spinal cord, thalamus, and somatosensory cortex, while AI-induced analgesia was associated with reversal of these expression changes. Further, upregulation of TRPV1-associated signaling factors was not observed in *Trpv1* knockout mice following CFA injection. In addition, the activated microglial markers Iba-1 and S100B demonstrated similar expression changes and were colocalized with TRPV1.

Conclusions: These findings suggest that AI can mitigate chronic pain (and sequel such as comorbid depression) by suppressing TRPV1 overexpression in neuronal or microglial cells.

Introduction

Acupoint injection (AI or prolotherapy) is increasing in popularity as a complementary therapy for chronic pain. The most common form involves the injection of a glucose solution to induce local inflammation and initiate a wound-healing cascade. Prolotherapy is often utilized for relief pain of ligaments, tendons, and articular cartilage. After injection of concentrated glucose, the damaged tissue is repaired to form a denser, stronger, and tighter ligament or tendon [1, 2]. In the clinic, prolotherapy is usually performed in 4–6 courses to ensure tissue repair and pain relief [3, 4]. Several other solutions have also been used for prolotherapy, including dextrose and phenol. Although prolotherapy has demonstrated efficacy for healing local tissue damage, the underlying mechanisms of action are still unclear. One possibility is that dextrose induces osmotic damage to local neurons, which in turn attracts brain-resident inflammatory mediators to initiate the wound-healing cascade [5]. Local osmotic damage may also induce the infiltration of granulocytes followed by monocytes and macrophages [6]. However, elucidation of the actual mechanisms requires the use of appropriate animal models.

Another potential mechanism involves the transient receptor potential vanilloid 1 (TRPV1) channel responsive to thermal, mechanical, and capsaicin stimulation and expressed by peripheral sensory neurons. Activation of TRPV1 channels triggers cation influx, including Ca^{2+}, which activates downstream

signaling pathways causing peripheral and central pain sensitization [7, 8]. Peripheral inflammation induced by painful (potentially tissue-damaging) stimulation and local injury may also enhance signal propagation from the periphery to somatosensory cortex via the dorsal root ganglion, spinal cord, and thalamus, termed central sensitization, leading to allodynia, a condition in which even light touch and other normally non-painful stimuli are perceived as painful [7, 8]. The TRPV1 channel and related downstream signaling molecules are involved in both acute pain and central sensitization, and TRPV1 was recently shown to detect neuroinflammation in mice [9, 10].

Acupuncture has been used for over 3,000 years to treat pain and associated disorders, and modern acupuncture techniques have proven to be convenient, safe, and inexpensive approaches for treating diseases [11–15]. These therapies are particularly beneficial for lower back pain, inflammatory pain, and muscle pain due to exercise, fibromyalgia (FM), and myofascial pain [16–20]. Recent studies have implicated release of adenosine [21], dopamine [22], and endogenous opiates [23] in the analgesic effects of acupuncture as evidenced by elevated levels in serum or cerebrospinal fluid.

In the current study, we examined the efficacy of AI against chronic inflammatory pain (CIP) and the underlying mechanisms. We hypothesized that AI of high concentration glucose would be effective for treating chronic mechanical and thermal hyperalgesia in mice by regulating TRPV1 signaling from periphery to somatosensory cortex.

Materials And Methods

2.1 Animals

We used 8–12 week old C57BL/6 mice for all experiments, which were purchased from BioLASCO Co. Ltd. (Taipei, Taiwan). The mice were randomly assigned to four groups (n = 8 per group): (1) Normal, (2) CIP, (3) CIP + AI, and (4) CIP + *Trpv1*$^{-/-}$. The sample size required for an alpha of 0.05 and a power of 80% was eight animals per group. After arrival, the mice were housed in a room under a 12/12 h light/dark cycle with water and food available *ad libitum*. All procedures were approved by the Institutional Animal Care and Use Committee of China Medical University (No. 2018 – 110) and were conducted in accordance with the Guide for the Use of Laboratory Animals provided by the National Research Council and the ethical guidelines of the International Association for the Study of Pain. The number of animals used and their suffering were minimized.

2.2 CIP induction

Mice were randomly divided into four groups and then anesthetized with 1% isoflurane for CFA injections and AI treatment. Mice were next injected with 20 µl saline (pH 7.4, buffered with 20mM HEPES) or CFA 20 µl (complete Freund's adjuvant; 0.5 mg/ml heat-killed M. tuberculosis (Sigma, St. Louis, MO) suspended in oil:saline 1:1 emulsion) in the plantar surface of the hind paw. CFA was used to induce intraplantar chronic inflammation. CFA were administered twice: at baseline and day 7. Four groups and their treatments were as follows: (1) normal group: anesthesia with normal saline injection; (2) CIP group:

anesthesia with CFA injections to induce CIP; (3) AI group: CIP mice treated with AI; and (4) *Trpv1*$^{-/-}$ group: CFA injections in *Trpv1*$^{-/-}$ mice.

2.3 Nociceptive behavioural examination

The mechanical and thermal pain behaviors were determined 3 times at day 0, day 7 and day 14 throughout the experiment after the induction of the CIP model. All mice were moved to the behavior analysis room, and were adapted to the environment for at least 30 min before behavior tests. All experiments were performed at room temperature and the stimuli were applied only when the animals were calm but not sleeping or grooming. First, the von Frey filament test was conducted. Mechanical sensitivity was measured by testing the force of responses to stimulation with 3 applications of the electronic, calibrated von Frey filament (IITC Life Science Inc., USA). Mice were placed onto a metal mesh (75x25x45 cm) and covered with a plexiglass cage (10x6x11 cm). Subjects were then mechanically stimulated by the tip of the filament at the plantar region of the right hind paw. The filament gram counts were recorded when the stimulation caused the subject to withdraw its hind paw. Second, the Hargreaves' assessment was used to measure thermal pain behavior by testing the time of response to thermal stimulation with 3 applications using Hargreaves' test IITC analgesiometer (IITC Life Sciences, SERIES8, Model 390G). The mice were placed in a plexiglass cage on top of a glass sheet. The thermal stimulator was positioned under the glass sheet and the focus of the projection bulb was aimed exactly at the middle of the plantar surface of the right hind paw. A cut-off time of 20s was set to prevent tissue damage. In the thermal paw withdrawal test, the nociception threshold was assessed using the latency of paw withdrawal upon stimulus, and was recorded when the constant applied heat stimulation caused the subject to withdraw its hindpaw.

2.4 Acupoint injection

AI was conducted in the morning (9:00–10:00 am) immediately after the induction of CIP. High concentration of glucose (20%, 20μL) was injected at the bilateral side of ST36 at baseline and day 7. Similar to humans, the ST36 point is located longitudinally at 3 cun below the knee joint and intersects with the middle of the tibialis anterior muscle. Mice were placed into a fixation machine under anesthesia with 5% isoflurane for induction, which was then decreased to 1% for maintenance. Bilateral ST36 acupoint were selected, sterilized with 70% alcohol and iodine solution and the glucose solution was injected at the 3–5 mm depth.

2.5 Tissue sampling and western blot analysis

The lumbar dorsal root ganglion (DRG), spinal cord (SC), full thalamus and somatosensory cortex (SSC) neurons were excised immediately to extract proteins. Total proteins were prepared by homogenizing the tissues in lysis buffer containing 50 mM Tris-HCl (pH 7.4), 250 mM NaCl, 1% NP-40, 5 mM EDTA, 50 mM NaF, 1 mM Na_3VO_4, 0.02% $NaNO_3$, and 1× protease inhibitor cocktail (Amresco, Solon, OH, USA). The extracted proteins (30 μg per sample according to the BCA protein assay) were subjected to 8% sodium dodecyl sulfate-Tris glycine gel electrophoresis and transferred to a PVDF membrane. The membrane was blocked with 5% non-fat milk in TBS-T buffer (10 mM Tris pH 7.5, 100 mM NaCl, 0.1% Tween 20),

incubated with a primary antibodies (1:1000, Alomone, Jerusalem, Israel): anti-tubulin, anti-TRPV1, anti-Nav1.7, anti-Nav1.8, anti-RAGE, anti-pmTOR, anti-pPI3K, anti-pAkt, anti-pERK, anti-pS100B, anti- pNFκB, anti-pCREB, anti-pPKC or anti-pPKA in TBS-T and 1% bovine serum albumin, and incubated for 1 h at room temperature. A peroxidase-conjugated anti-rabbit antibody (1:5,000) was used as the secondary antibody. The bands were visualized using an enhanced chemiluminescent substrate kit (Pierce, Rockford, IL, USA) with LAS-3000 Fujifilm (Fuji Photo Film Co. Ltd., Tokyo, Japan). If appropriate, the image intensities of specific bands were quantified with NIH ImageJ software (Bethesda, MD, USA). The protein ratios were determined by dividing the target protein intensities by the intensity of α-tubulin or β-actin (internal control) in the same sample. The calculated ratios were adjusted by dividing the ratios from the same comparative group relative to the control.

2.6 Immunofluorescence

Mice were euthanized with a 5% isoflurane via inhalation and intracardially perfused with normal saline followed by 4% paraformaldehyde. The brain was immediately dissected and post fixed with 4% paraformaldehyde at 4 ºC for 3 days. The tissues were placed in 30% sucrose for cryoprotection overnight at 4 ºC. The brain was embedded in an Optimal cutting temperature (OCT) compound and rapidly frozen using liquid nitrogen before storing the tissues at -80 ºC. Frozen segments were cut at 20-μm width on a cryostat then instantaneously placed on glass slides. The samples were fixed with 4% paraformaldehyde, and then incubated with a blocking solution, consisting of 3% BSA, 0.1% Triton X-100, and 0.02% sodium azide, for 1 h at room temperature. After blocking, the samples were incubated with the primary antibody (1:200, Alomone), TRPV1 and Iba1, prepared in 1% bovine serum albumin solution at 4ºC overnight. The samples were then incubated with the secondary antibody (1:500), 488-conjugated AffiniPure donkey anti-rabbit IgG (H + L), 594-conjugated AffiniPure donkey anti-goat IgG (H + L) and Peroxidase-conjugated AffiniPure donkey anti-mouse IgG (H + L) for 2 h at room temperature before being fixed with cover slips for immunofluorescence visualization. The samples were observed by an epi-fluorescent microscope (Olympus, BX-51, Japan) with 20 x numerical aperture (NA = 1.4) objective. The images were analyzed by NIH Image J software (Bethesda, MD, USA).

2.7 Statistical analysis

Statistical analysis was performed using the SPSS statistic program. All of the data were expressed as the mean ± standard error (SEM). Shapiro-Wilk test was performed to test the normality of data. Significant differences among all groups were tested using the repeated measure ANOVA, followed by a post hoc Tukey's test. $p < 0.05$ was considered significantly different.

Results

3.1 AI treatment suppresses TRPV1-dependent mechanical and thermal hyperalgesia

We used von Frey filaments to assess mechanical sensitivity and Hargreaves' test to assess thermal sensitivity at baseline, after injection of CFA to induce CIP, and following either control treatment or AI. At baseline (day 0), there were no significant differences in von Frey filament or Hargreaves' thermal test

sensitivity among treatment groups. One week after CIP induction, however, mechanical sensitivity was significantly elevated in the CIP group compared to the sham treatment group, indicating hyperalgesia (Fig. 1A, red column, n = 8). This mechanical hyperalgesia was significantly reversed by AI treatment (CIP + AI group) (Fig. 1A, blue column, n = 8 mice). Similar to CIP + AI group mice, *Trpv1*$^{-/-}$ mice (Fig. 1A, green column, n = 8 mice) also exhibited little mechanical hyperalgesia following CIP. Thus, the hyperalgesic effects of CIP and the anti-hyperalgesic effects of AI appear to depend on modulation of TRPV1 channels.

3.2 Effects of CIP and AI on the expression levels of TRPV1 and associated signaling molecules in mouse dorsal root ganglia and spinal cord

To examine the involvement of TRPV1 channels and related signaling factors in hyperalgesia and AI-mediated analgesia, changes in expression were examined by western blotting of DRG and SC tissue samples isolated after successful induction of hyperalgesia by CIP and reversal by AI (as confirmed by von Fey and Hargreaves' tests). In the DRG (Fig. 2), TRPV1 protein expression was significantly increased by CIP induction compared to sham-treated controls, and this augmentation was significantly reversed by AI. In addition, expression levels of phosphorylated (activated) PKA (pPKA) (Fig. 2B), pPI3K (Fig. 2C), and pPKC (Fig. 2D) were significantly elevated in the DRG after CIP, and these responses were attenuated by AI. Increased expression levels were also attenuated following CIP in *Trpv1*$^{-/-}$ mice compared to wild type (WT) mice (CIP group). In addition, DRG expression levels of the phospho-activated mitogen activated protein kinases (MAPKs) pERK (Fig. 2E), pJNK (Fig. 2F), and pp38 (Fig. 2G) were elevated in CIP model mice, and these effects were reversed by AI and lower in *Trpv*1$^{-/-}$ mice than WT mice following CIP induction. Expression levels of pAkt (Fig. 2H) and pmTOR Fig. 2I), two downstream effectors of pPI3K, and of the transcription factors pCREB (Fig. 2J) and NFκB (Fig. 2K) were upregulated during CIP, reversed by AI, and lower following CIP in *Trpv*1 KO mice than WT mice. The nociception-associated Na channel subunits Nav1.7 (Fig. 2L) and Nav1.8 (Fig. 2M) demonstrated similar patterns of expression change. Finally, the activated microglial markers Iba1 (Fig. 2N), S100B (Fig. 2O), and RAGE (Fig. 2P) were also elevated by CIP, and these responses were reversed by AI and lower in CIP model *Trpv*1$^{-/-}$ mice than CIP model WT mice. Collectively, these findings suggest that CIP was induced by activated microglia. Similar changes in protein expression were also observed in tissue samples from the SC (Fig. 3).

3.3 Increased TRPV1 and associated protein levels following CIP induction, reversal by AI, and suppression by *Trpv1* gene deletion in thalamus and somatosensory cortex

Samples of thalamus (Fig. 4) and somatosensory cortex (Fig. 5) were also examined by western blotting for changes in the expression levels of TRPV1 and downstream signaling molecules following CIP induction and AI. In accord with findings in DRG and SC, there were significant increases in the expression levels of TRPV1 (Fig. 4A, 5A), pPKA (Fig. 4B, 5B), pPI3K (Fig. 4C, 5C), pPKC (Fig. 4D, 5D), pERK (Fig. 4E, 5E), pJNK (Fig. 4F, 5F), pp38 (Fig. 4G, 5G), pAkt (Fig. 4H, 5H), pmTOR (Fig. 4I, 5I), pCREB (Fig. 4J, 5J), pNFκB (Fig. 4K, 5K), Nav1.7 (Fig. 4L, 5L), Nav1.8 (Fig. 4M, 5M), Iba1 (Fig. 4N, 5N), S100B (Fig. 4O, 5O), and RAGE (Fig. 4P, 5P) following CIP induction. Also in accord with findings in the DRG, these changes

were attenauted by AI and lower in CIP model *Trpv1*$^{-/-}$ mice than WT mice, suggesting that induced hyperalgesia and reversal by AI are dependent on modulation of TRPV1 expression and downstream signaling pathways.

3.4 Co-expression of TRPV1 and Iba1 in DRG and SC
To examine the cellular elements responsible for these expression changes, we conducted immunofluorescence staining of the DRG (Fig. 6) and somatosensory cortex (Fig. 7). Immunofluorescence images of the DRG revealed changes in TRPV1 immunoexpression that paralleled those measured by western blotting, with elevation following CIP induction compared to sham control mice and markedly lower expression levels in CIP + AI and CIP + KO groups (Fig. 6A). Immunofluorescence staining also confirmed elevated expression of the glial cell marker Iba1 in the DRG following CIP induction, which was attenuated by AI treatment and *Trpv1* gene deletion (Fig. 6B). Further, TRPV1 and Iba1 were colocalized in CIP model mice, indicating that the elevation in tissue TRPV1 was mediated by increased expression in DRG glial cells. Consistent with western blotting results, this increase was reversed in CIP + AI and *Trpv1* KO mice (Fig. 6C). Similar changes in TRPV1 and Iba1 expression were also observed in the somatosensory cortex (Fig. 7).

3.5 Co-expression of TRPV1 and Iba1 in cells of thalamus and somatosensory cortex
Finally, we examined these changes in cellular TRPV1 and Iba1 in thalamus (Fig. 8) and somatosensory cortex (Fig. 9). In accord with western blotting and other immunofluorescence results, TRPV1 immunoreactivity (Fig. 8A) and Iba1 immunoreactivity (Fig. 8B) were elevated concomitantly by CIP induction. Further, these elevated expression levels were reversed by AI (Fig. 8A and 8B, respectively), while Iba1 expression was lower in CIP model *Trpv1* KO mice than WT mice (Fig. 8C). In the somatosensory cortex as well, TRPV1, Iba1, and TRPV1/Iba1 co-staining signals were all increased in CIP model mice and reversed by AI (Fig. 9). Further, the changes in Iba1 were suppressed in *Trpv1*$^{-/-}$ mice.

Discussion

In the present study, we present evidence that the hyperalgesia induced by CFA and the analgesic efficacy of AI are dependent on reciprocal modulation of TRPV1 channels expressed by glial cells in the DRG, SC, thalamus, and somatosensory cortex. Two weeks after CFA injection, mice demonstrated both mechanical hyperalgesia as evidence by increased von Frey filament sensitivity and thermal hyperalgesia as evidenced by Hargreaves' thermal response test, and these changes were associated with upregulation of TRPV1 channels, a myriad of downstream kinases and transcription factors, and voltage-gated sodium channels (Na_vs). Conversely, both forms of hyperalgesia were suppressed by AI treatment concomitant with reduced expression of TRPV1, associated signaling molecules, and Na_vs. Further, these hyperalgesia-associated increases in downstream signaling molecules and Na_vs were markedly suppressed by *Trpv1* KO. Expression levels of the activated microglial markers Iba1 and S100B were also upregulated by CIP induction, and these responses were reversed by AI. Collectively, these findings

indicate that TRPV1 signaling in microglia is a major driver of CFA-induced hyperalgesia and a primary therapeutic target of AI.

The TRPV1 is also implicated in ST36 acupoint treatment, suggesting crucial involvement in the neurobiology of chronic pain and clinical potential as a treatment target [16]. Influx of cations, particularly Ca^{2+}, through TRPV1 channels activates the PI3K/Akt/mTOR and MAPK signaling pathways [24–27], and simultaneous overexpression of PKA, PI3K, PKC, ERK, Akt, and mTOR has been observed in various chronic pain states, while reversal of overexpression has been observed after successful acupuncture [28]. Among transcription factors implicated in clinical pain conditions, CREB and pNFκB appear to mediate the gene expression changes observed in CIP model mice. Overexpression of the voltage-gated sodium channels Nav1.7 and Nav1.8 have also been observed in the DRG and SC of acute pain model animals [29]. Conversely, suppression of Nav1.7 was associated with long-lasting analgesia [30]. Furthermore, Nav1.8 is highly expressed by nociceptive sensory afferents, and expression increases during chronic pain [31]. The present study provides evidence that AI of glucose alleviates mechanical and thermal hyperalgesia by suppressing this increase in Nav1.8 through downregulation of TRPV1 signaling in both PNS and CNS glial cells.

A recent study by He et al. (2017) provided evidence that nociceptive neuropeptides such as SP, CGRP and 5-HT are highly expressed at acupoints [32], implicating modulation of these signaling pathways in AI-induced analgesia. Increased excitability of DRG neurons has been linked to overexpression of a hyperpolarization-activated cyclic nucleotide-gated channel [33], and Zhang et al. (2019) reported that sensitization was associated with increased HCN2 channel expression and ensuing hyperexcitability of C fiber neurons [34]. Huang et al. (2018) also suggested that mast cells are crucial components of acupoints and can be activated by TRPV2 channels during acupuncture. These mast cells then activate either histamine H1 or adenosine A1 receptors, which underlie the acupuncture response [35]. Li et al. (2019) reported that lipopolysaccharide (LPS)-induced lung inflammation associated with increased expression of the proinflammatory cytokines TNF-α and IL-6, and decreased expression of the antioxidant superoxide dismutase (SOD), could be effectively alleviated by acupoint catgut embedding [36]. Chao et al. also reported that AI of vitamin K at SP6 increased plasma vitamin K in dysmenorrhea patients, and that a higher vitamin K concentration was correlated with greater pain suppression [37]. A randomized, double-blinded, placebo-controlled clinical trial found that AI of onabotulinum toxin A (BoNTA) was more effective at suppressing pain than muscle injection in rats. They further suggested that BoNTA may suppress migraine through changes in CGRP and SP release within the medulla oblongata, possibly via a SNAP-dependent mechanism [38]. Ji et al. also reported that acupoint gel embedding could significantly diminish myocardial infarcted size and inflammatory responses via the Notch-1signaling pathway [39]. Our results extend the potential mechanisms underlying the benefits of AI to include analgesia via modulation of glial TRPV1 expression and signaling.

Conclusion

In summary, the present study indicates that CFA can reliably induced CIP via upregulation of TRPV1 signaling and that AI can suppress CIP by reversing this upregulation. In addition, the activated microglial markers Iba-1 and S100B demonstrated similar expression changes and were colocalized with TRPV1. These findings suggest that AI can mitigate chronic pain by suppressing TRPV1 overexpression in both neuronal and microglial cells.

Abbreviations

TRPV1: Transient Receptor Potential V1

DRG: Dorsal Root Ganglion

SC: Spinal cord

SSC: Somatosensory Cortex

RAGE: Receptor for Advanced Glycation End-products

TNF-α: Tumor Necrosis Factor-α

NFkB: Nuclear Factor kappa-light-chain-enhancer of activated B cells

ERK: Extracellular signal-Regulated protein Kinase

JNK: c-Jun N-terminal Kinase/stress-activated protein kinase

AI: Acupoint Injection

CIP: Chronic Inflammatory Pain

Declarations

Ethics approval and consent to participate

All ethics are approved and consent to participate in this manuscript.

Consent for publication

All authors have read the manuscript and consent for publication.

Availability of data and materials

The datasets supporting the conclusions of this article are included within the article.

Conflict of Interest

There are no financial or other relationships that might lead to a conflict of interest for all authors.

Funding

This work was supported by the following grants: MOST 108-2320-B-039-028-MY3, DMR-110-193 and the "Chinese Medicine Research Center, China Medical University" from The Featured Areas Research Center Program within the framework of the Higher Education Sprout Project by the Ministry of Education (MOE) in Taiwan.

Authors' contributions

Hsien-Yin Liao: Conceptualization, Methodology. Ming-Chia Lin: Software, Data curation.: Hsien-Yin Liao: Writing - original draft, Visualization, Investigation. Yi-Wen Lin: Supervision, Validation, Writing - review & editing

Acknowledgements

The authors would like to thank Enago (www.enago.tw) for the English language review

References

1. Chung MW, Hsu CY, Chung WK, Lin YN. Effects of dextrose prolotherapy on tendinopathy, fasciopathy, and ligament injuries, fact or myth?: A systematic review and meta-analysis. Medicine. 2020;99(46):e23201.
2. Nuhmani S. Injection therapies for patellar tendinopathy. The Physician sportsmedicine. 2020;48(2):125–30.
3. Rabago D, Nourani B. Prolotherapy for Osteoarthritis and Tendinopathy: a Descriptive Review. Curr Rheumatol Rep. 2017;19(6):34.
4. Reeves KD, Sit RW, Rabago DP. Dextrose Prolotherapy: A Narrative Review of Basic Science, Clinical Research, and Best Treatment Recommendations. Phys Med Rehabil Clin North Am. 2016;27(4):783–823.
5. Siadat AH, Isseroff RR. Prolotherapy: Potential for the Treatment of Chronic Wounds? Advances in wound care 2019; 8 (4): 160–167.
6. Jensen KT, Rabago DP, Best TM, Patterson JJ, Vanderby R. Jr. Early inflammatory response of knee ligaments to prolotherapy in a rat model. Journal of orthopaedic research: official publication of the Orthopaedic Research Society. 2008;26(6):816–23.
7. Frias B, Merighi A. Capsaicin. Nociception and Pain. Molecules 2016; 21 (6).
8. Caterina MJ, Leffler A, Malmberg AB, Martin WJ, Trafton J, Petersen-Zeitz KR, et al. Impaired nociception and pain sensation in mice lacking the capsaicin receptor. Science. 2000;288(5464):306–13.

9. Kong WL, Peng YY, Peng BW. Modulation of neuroinflammation: Role and therapeutic potential of TRPV1 in the neuro-immune axis. Brain Behav Immun. 2017;64:354–66.
10. Lin YW, Chou AIW, Su H, Su KP. Transient receptor potential V1 (TRPV1) modulates the therapeutic effects for comorbidity of pain and depression: The common molecular implication for electroacupuncture and omega-3 polyunsaturated fatty acids. Brain Behav Immun. 2020;89:604–14.
11. Zhang C, Xia C, Zhang X, Li W, Miao X, Zhou Q. Wrist-ankle acupuncture attenuates cancer-induced bone pain by regulating descending pain-modulating system in a rat model. Chin Med. 2020;15:13.
12. Jeon J, Bussin E, Scott A. Temporal divergence of changes in pain and pain-free grip strength after manual acupuncture or electroacupuncture: an experimental study in people with lateral epicondylalgia. Chinese medicine 2017; 12 22.
13. Zhang YJ, Cao HJ, Li XL, Yang XY, Lai BY, Yang GY, et al. Cupping therapy versus acupuncture for pain-related conditions: a systematic review of randomized controlled trials and trial sequential analysis. Chinese medicine 2017; 12 21.
14. Itoh K, Minakawa Y, Kitakoji H. Effect of acupuncture depth on muscle pain. Chin Med. 2011;6(1):24.
15. Moskvin S, Pritiko D, Sergeenko E, Lukash E, Gusev L. A brief literature review and own clinical experience in prophylaxis of oral mucositis in children using low level laser therapy. BioMedicine. 2019;9(1):1.
16. Wu SY, Chen WH, Hsieh CL, Lin YW. Abundant expression and functional participation of TRPV1 at Zusanli acupoint (ST36) in mice: mechanosensitive TRPV1 as an "acupuncture-responding channel". BMC Complement Altern Med. 2014;14:96.
17. Huang HY, Liao HY, Lin YW. Effects and Mechanisms of Electroacupuncture on Chronic Inflammatory Pain and Depression Comorbidity in Mice. Evidence-based complementary and alternative medicine: eCAM 2020; 2020 4951591.
18. Yen CM, Wu TC, Hsieh CL, Huang YW, Lin YW. Distal Electroacupuncture at the LI4 Acupoint Reduces CFA-Induced Inflammatory Pain via the Brain TRPV1 Signaling Pathway. Int J Mol Sci. 2019;20:(18).
19. Liao HY, Hsieh CL, Huang CP, Lin YW. Electroacupuncture Attenuates Induction of Inflammatory Pain by Regulating Opioid and Adenosine Pathways in Mice. Scientific reports. 2017;7(1):15679.
20. Yen LT, Hsieh CL, Hsu HC, Lin YW. Targeting ASIC3 for Relieving Mice Fibromyalgia Pain: Roles of Electroacupuncture, Opioid, and Adenosine. Scientific reports. 2017;7:46663.
21. Goldman N, Chen M, Fujita T, Xu Q, Peng W, Liu W, et al. Adenosine A1 receptors mediate local anti-nociceptive effects of acupuncture. Nature neuroscience. 2010;13(7):883–8.
22. Torres-Rosas R, Yehia G, Pena G, Mishra P, del Rocio Thompson-Bonilla M, Moreno-Eutimio MA, et al. Dopamine mediates vagal modulation of the immune system by electroacupuncture. Nature medicine. 2014;20(3):291–5.
23. Ishikawa S, Suga H, Fukushima M, Yoshida A, Yoshida Y, Sunagawa M, et al. Blood fluidity enhancement by electrical acupuncture stimulation is related to an adrenergic mechanism. J Acupunct Meridian Stud. 2012;5(1):21–8.

24. Carbone E. Noradrenergic inhibition of presynaptic TRPV1 channels: a new pathway of pain control. J Physiol. 2017;595(8):2413–4.
25. Storozhuk MV, Moroz OF, Zholos AV. Multifunctional TRPV1 Ion Channels in Physiology and Pathology with Focus on the Brain, Vasculature, and Some Visceral Systems. BioMed research international 2019; 2019 5806321.
26. Zhuang ZY, Xu H, Clapham DE, Ji RR. Phosphatidylinositol 3-kinase activates ERK in primary sensory neurons and mediates inflammatory heat hyperalgesia through TRPV1 sensitization. The Journal of neuroscience: the official journal of the Society for Neuroscience. 2004;24(38):8300–9.
27. Inprasit C, Huang YC, Lin YW. Evidence for acupoint catgut embedding treatment and TRPV1 gene deletion increasing weight control in murine model. Int J Mol Med. 2020;45(3):779–92.
28. Lottering B, Lin YW. Functional characterization of nociceptive mechanisms involved in fibromyalgia and electroacupuncture. Brain research. 2021;1755:147260.
29. Inprasit C, Lin YW. TRPV1 Responses in the Cerebellum Lobules V, VIa and VII Using Electroacupuncture Treatment for Inflammatory Hyperalgesia in Murine Model. International journal of molecular sciences 2020; 21 (9).
30. Moreno AM, Aleman F, Catroli GF, Hunt M, Hu M, Dailamy A, et al. Long-lasting analgesia via targeted in situ repression of NaV1.7 in mice. Science translational medicine. 2021;13:(584).
31. Laird JM, Souslova V, Wood JN, Cervero F. Deficits in visceral pain and referred hyperalgesia in Nav1.8 (SNS/PN3)-null mice. The Journal of neuroscience: the official journal of the Society for Neuroscience. 2002;22(19):8352–6.
32. He W, Wang XY, Shi H, Bai WZ, Cheng B, Su YS, et al. Cutaneous neurogenic inflammation in the sensitized acupoints induced by gastric mucosal injury in rats. BMC Complement Altern Med. 2017;17(1):141.
33. Sun W, Yang F, Wang Y, Fu H, Yang Y, Li CL, et al. Contribution of large-sized primary sensory neuronal sensitization to mechanical allodynia by upregulation of hyperpolarization-activated cyclic nucleotide gated channels via cyclooxygenase 1 cascade. Neuropharmacology. 2017;113(Pt A):217–30.
34. Zhang M, Guo H, Ma Y, Xu F, Bai F, Liang S, et al. Acupoint Sensitization is Associated with Increased Excitability and Hyperpolarization-Activated Current (Ih) in C- But Not Adelta-Type Neurons. Neuroscience. 2019;404:499–509.
35. Huang M, Wang X, Xing B, Yang H, Sa Z, Zhang D, et al. Critical roles of TRPV2 channels, histamine H1 and adenosine A1 receptors in the initiation of acupoint signals for acupuncture analgesia. Scientific reports. 2018;8(1):6523.
36. Li D, Sun T, Chi L, Zhao D, Li W. Acupoint Catgut Embedding Improves the Lipopolysaccharide-Induced Acute Respiratory Distress Syndrome in Rats. BioMed research international 2020; 2020 2394734.
37. Chao MT, Wade CM, Booth SL. Increase in plasma phylloquinone concentrations following acupoint injection for the treatment of primary dysmenorrhea. J Acupunct Meridian Stud. 2014;7(3):151–4.

38. Hou M, Xie JF, Kong XP, Zhang Y, Shao YF, Wang C, et al. Acupoint injection of onabotulinumtoxin A for migraines. Toxins. 2015;7(11):4442–54.
39. Ji C, Song F, Huang G, Wang S, Liu H, Liu S, et al. The protective effects of acupoint gel embedding on rats with myocardial ischemia-reperfusion injury. Life sciences. 2018;211:51–62.

Figures

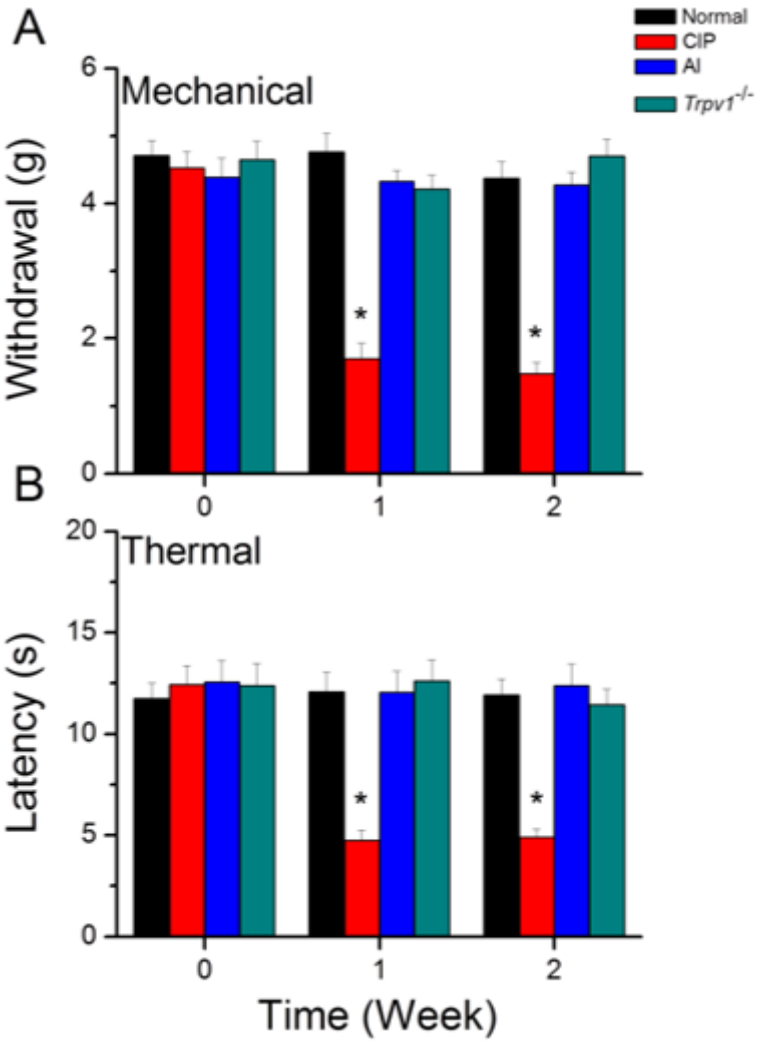

Figure 1

Mechanical withdrawal threshold and thermal latency in four groups of mice. Normal saline injection (Normal group, n = 8), CIP (CFA-induced CIP), AI (CFA-induced CIP with AI), and Trpv1-/- (CFA-induced CIP in Trpv1-/- mice). *p < 0.05 vs. Normal group.

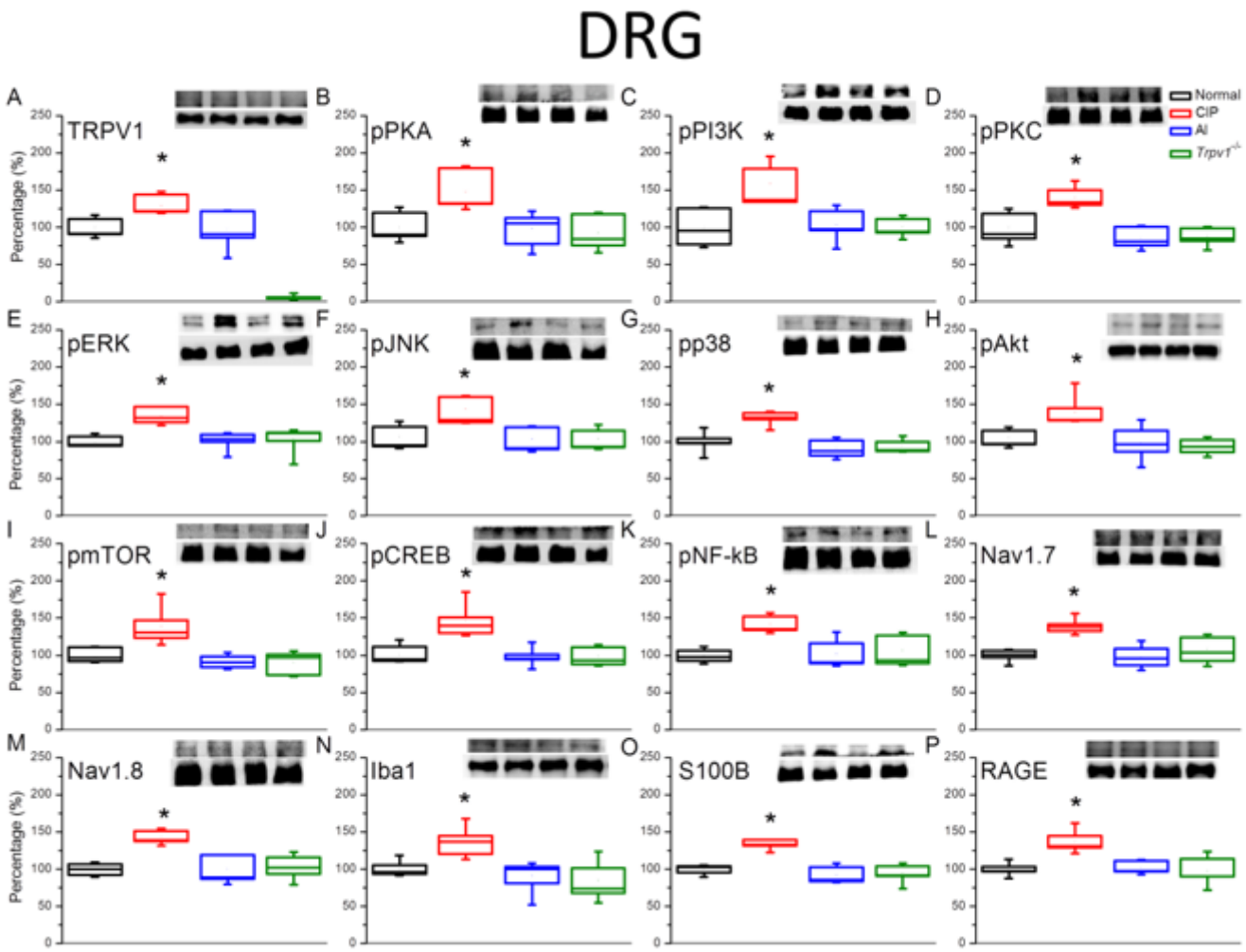

Figure 2

The expression levels of TRPV1 and associated molecules in the mice DRG. The immunoblotting images depict four lanes of protein in the following order: Normal, CIP, CIP + AI, CIP + KO groups. There are significant increases in protein expression in the CIP groups of (A) TRPV1, (B) pPKA, (C) pPI3K, (D) pPKC, (E) pERK, (F) pJNK, (G) pp38, (H) pAkt, (I) pmTOR, (J) pCREB, (K) pNFKB, (L) Nav1.7, (M) Nav1.8, (N) Iba1, (O) S100B, and (P) RAGE levels, which were significantly attenuated in the CIP + AI and AS + KO groups, depicting no difference when compared to the Normal group. * $p < 0.05$ means statistically difference. The western blot bands at the top show the target protein. The lower bands are internal controls (β-actin or α-tubulin).

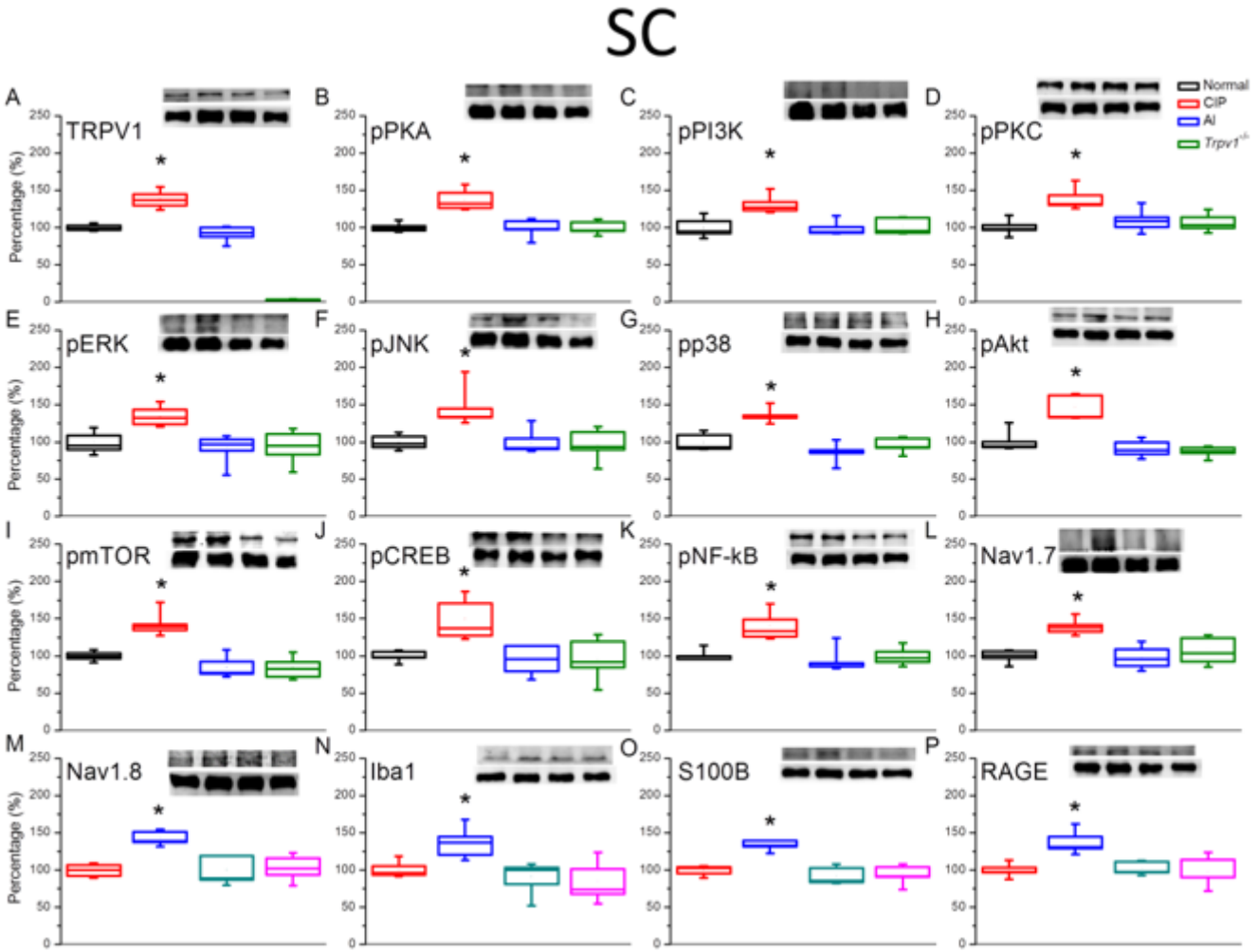

Figure 3

The expression levels of TRPV1 and associated molecules in the mice SC. The immunoblotting images depict four lanes of protein in the following order: Normal, CIP, CIP + AI, CIP + KO groups. There are significant increases in protein expression in the CIP groups of (A) TRPV1, (B) pPKA, (C) pPI3K, (D) pPKC, (E) pERK, (F) pJNK, (G) pp38, (H) pAkt, (I) pmTOR, (J) pCREB, (K) pNFKB, (L) Nav1.7, (M) Nav1.8, (N) Iba1, (O) S100B, and (P) RAGE levels, which were significantly attenuated in the CIP + AI and AS + KO groups, depicting no difference when compared to the Normal group. * $p < 0.05$ means statistically difference. The western blot bands at the top show the target protein. The lower bands are internal controls (β-actin or α-tubulin).

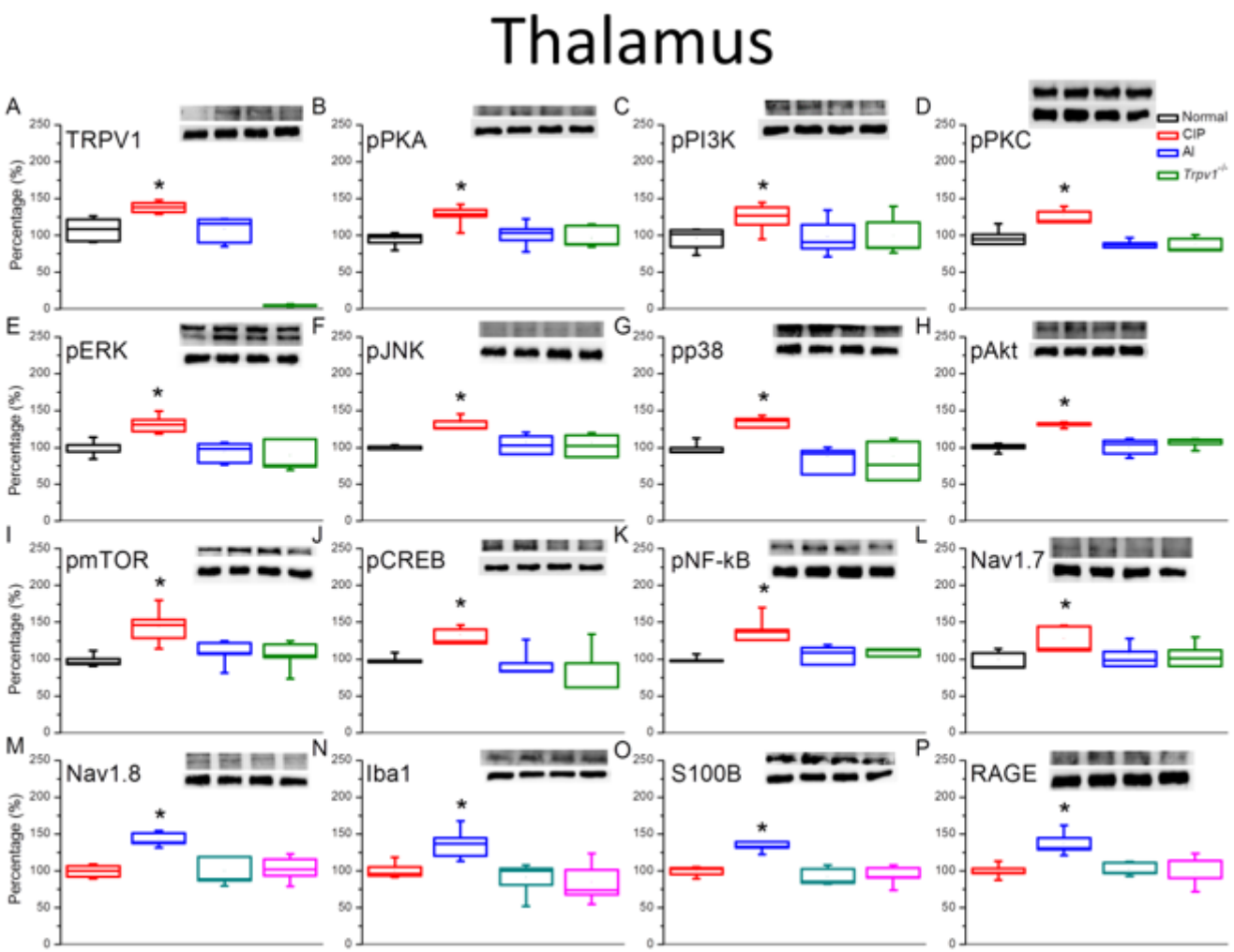

Figure 4

The expression levels of TRPV1 and associated molecules in the mice thalamus. The immunoblotting images depict four lanes of protein in the following order: Normal, CIP, CIP + AI, CIP + KO groups. There are significant increases in protein expression in the CIP groups of (A) TRPV1, (B) pPKA, (C) pPI3K, (D) pPKC, (E) pERK, (F) pJNK, (G) pp38, (H) pAkt, (I) pmTOR, (J) pCREB, (K) pNFKB, (L) Nav1.7, (M) Nav1.8, (N) Iba1, (O) S100B, and (P) RAGE levels, which were significantly attenuated in the CIP + AI and AS + KO groups, depicting no difference when compared to the Normal group. * $p < 0.05$ means statistically difference. The western blot bands at the top show the target protein. The lower bands are internal controls (β-actin or α-tubulin).

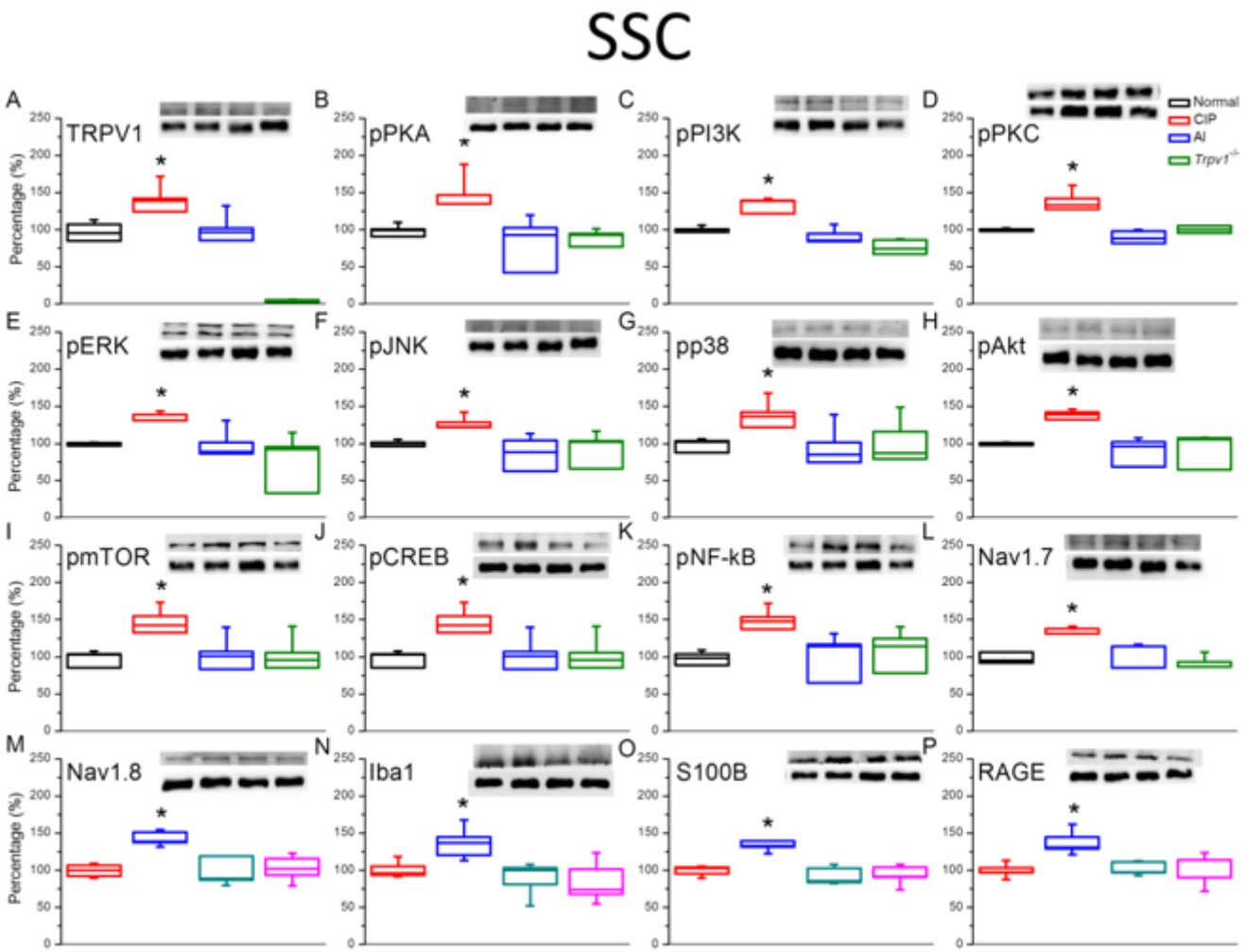

Figure 5

The expression levels of TRPV1 and associated molecules in the mice SSC. The immunoblotting images depict four lanes of protein in the following order: Normal, CIP, CIP + AI, CIP + KO groups. There are significant increases in protein expression in the CIP groups of (A) TRPV1, (B) pPKA, (C) pPI3K, (D) pPKC, (E) pERK, (F) pJNK, (G) pp38, (H) pAkt, (I) pmTOR, (J) pCREB, (K) pNFKB, (L) Nav1.7, (M) Nav1.8, (N) Iba1, (O) S100B, and (P) RAGE levels, which were significantly attenuated in the CIP + AI and AS + KO groups, depicting no difference when compared to the Normal group. * $p < 0.05$ means statistically difference. The western blot bands at the top show the target protein. The lower bands are internal controls (β-actin or α-tubulin).

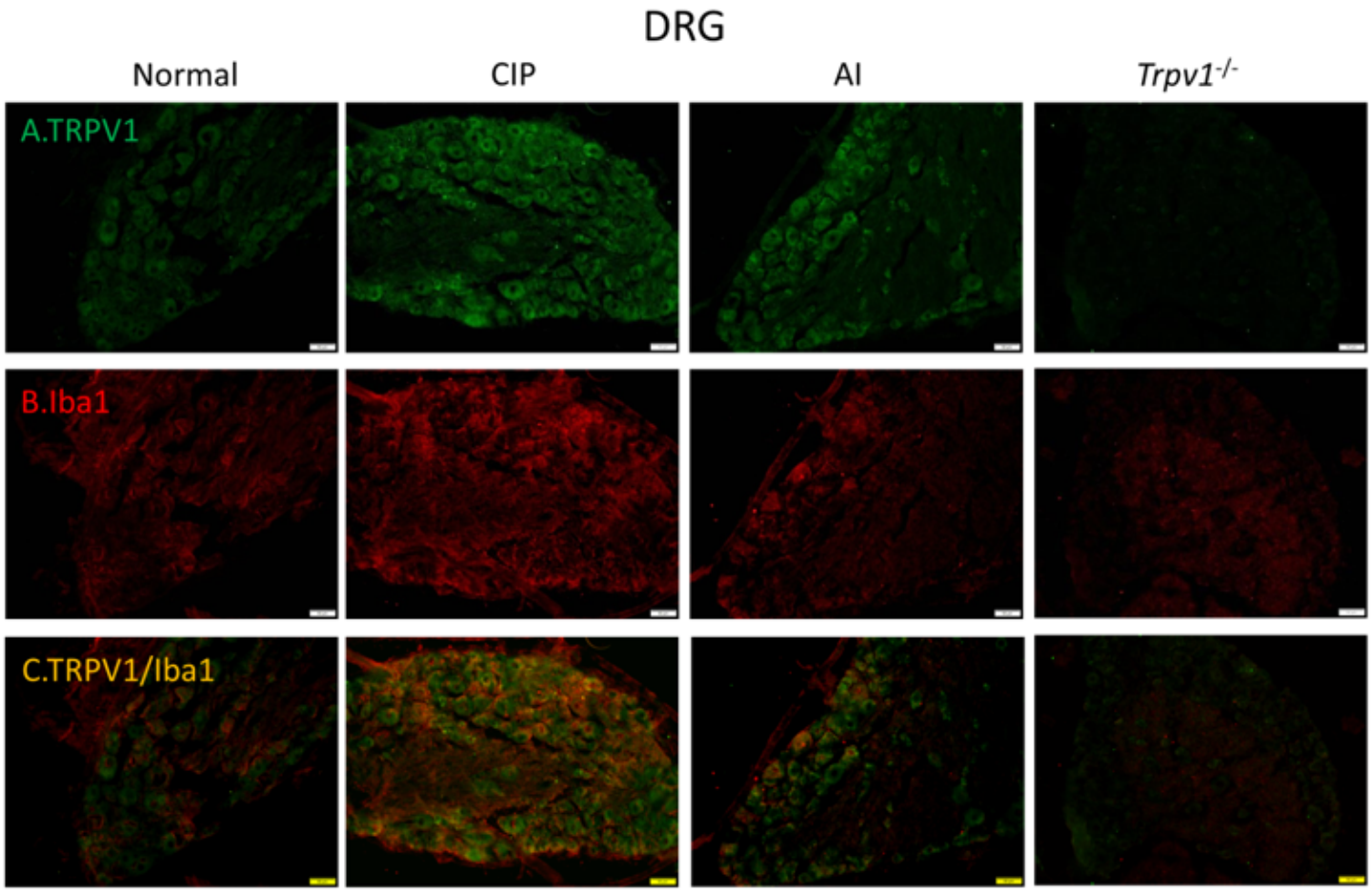

Figure 6

Immunofluorescence staining of TRPV1 and Iba1 protein expression in the mice DRG. There are 4 groups as: Normal, CIP, CIP + AI, and CIP + KO. (A) The efficacy of CIP treatment involves significant increase of TRPV1 (green) in the mice DRG. (B) Significant increase of Iba1 (red) of CIP treatment in the mice DRG. (C) Overexpression of co-localization of TRPV1 and Iba1 (yellow) in the mice DRG. Scale bar is 50 μm.

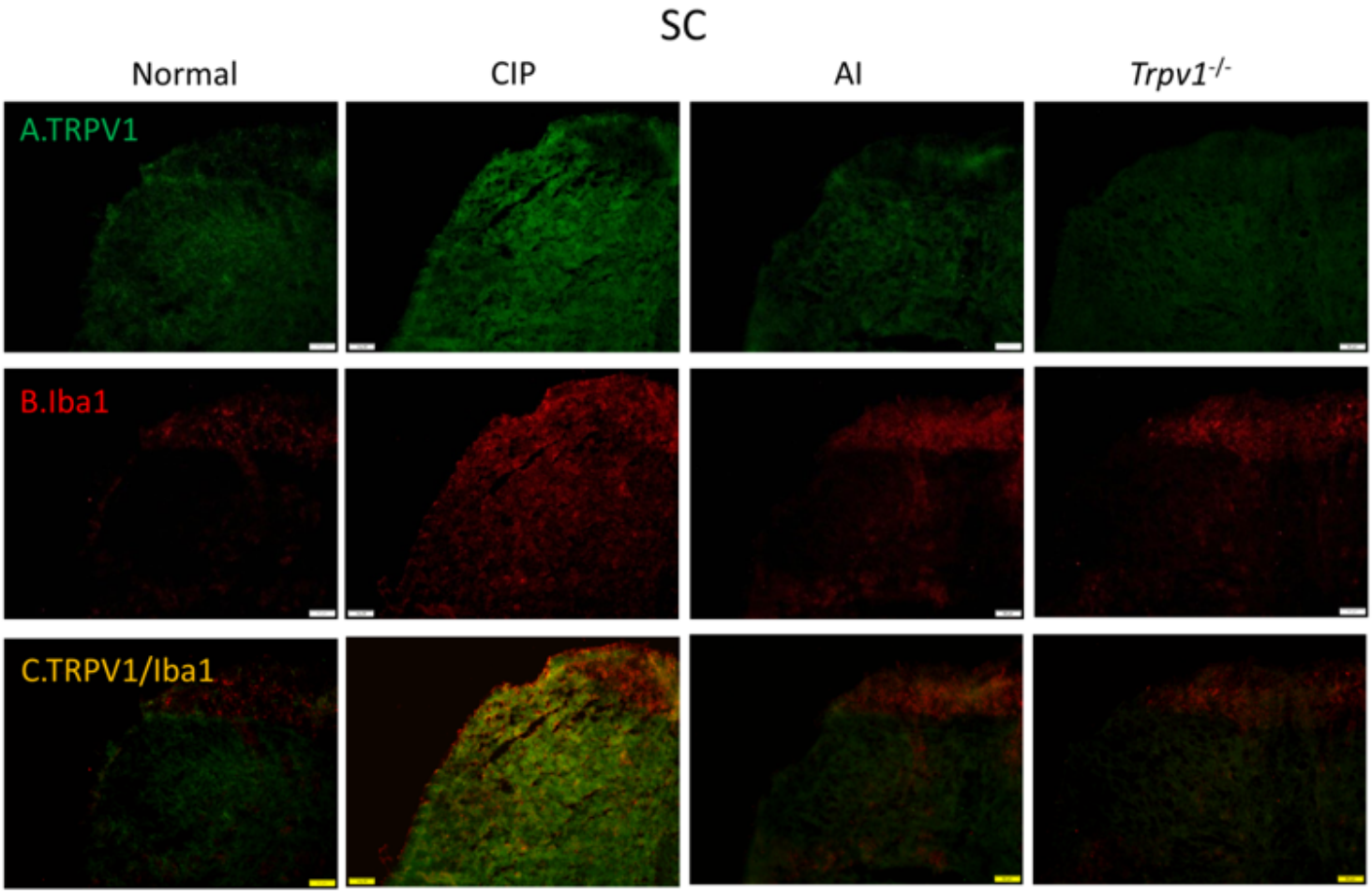

Figure 7

Immunofluorescence staining of TRPV1 and Iba1 protein expression in the mice SC. There are 4 groups as: Normal, CIP, CIP + AI, and CIP + KO. (A) The efficacy of CIP treatment involves significant increase of TRPV1 (green) in the mice DRG. (B) Significant increase of Iba1 (red) of CIP treatment in the mice DRG. (C) Overexpression of co-localization of TRPV1 and Iba1 (yellow) in the mice DRG. Scale bar is 50 μm.

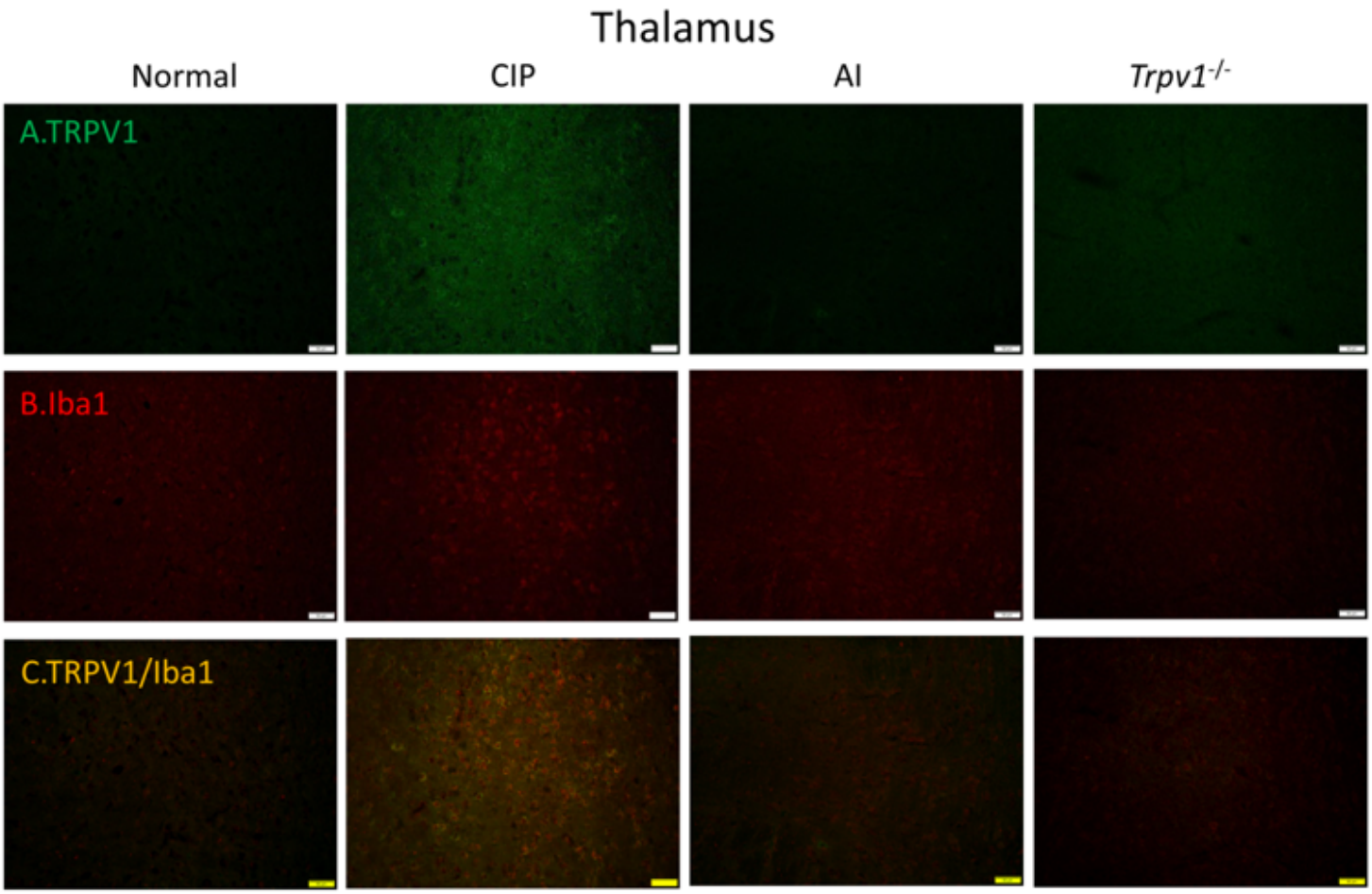

Figure 8

Immunofluorescence staining of TRPV1 and Iba1 protein expression in the mice thalamus. There are 4 groups as: Normal, CIP, CIP + AI, and CIP + KO. (A) The efficacy of CIP treatment involves significant increase of TRPV1 (green) in the mice DRG. (B) Significant increase of Iba1 (red) of CIP treatment in the mice DRG. (C) Overexpression of co-localization of TRPV1 and Iba1 (yellow) in the mice DRG. Scale bar is 50 μm.

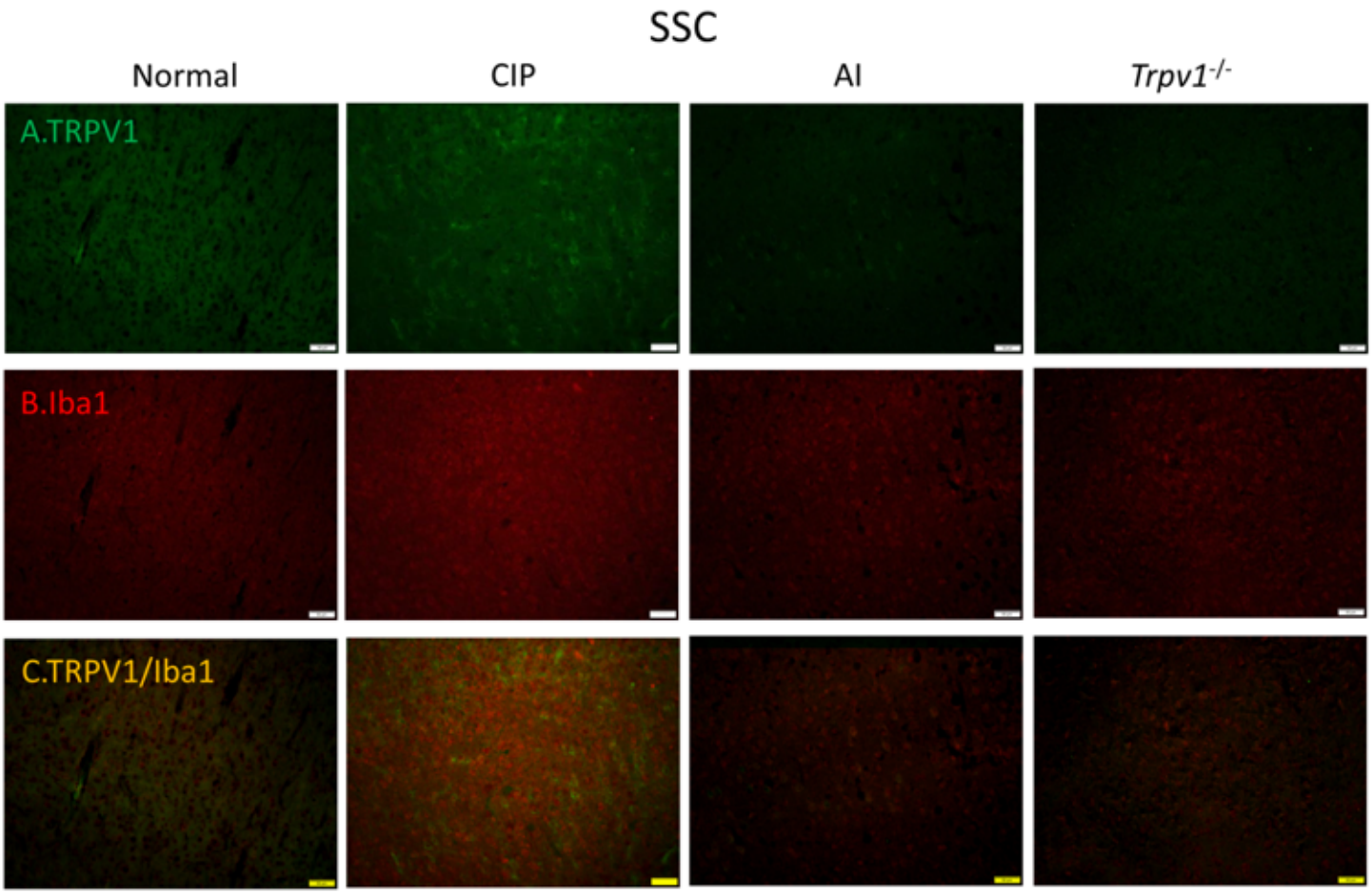

Figure 9

Immunofluorescence staining of TRPV1 and Iba1 protein expression in the mice SSC. There are 4 groups as: Normal, CIP, CIP + AI, and CIP + KO. (A) The efficacy of CIP treatment involves significant increase of TRPV1 (green) in the mice DRG. (B) Significant increase of Iba1 (red) of CIP treatment in the mice DRG. (C) Overexpression of co-localization of TRPV1 and Iba1 (yellow) in the mice DRG. Scale bar is 50 μm.